assembly may be required to locate the focal line precisely on the goniometer radius. The experiment also effectively measures the size of the focal line, in our case this was 0.15 mm. A slit of this dimension was fabricated, and the *x*–*y* translator was replaced with a standard slit retainer positioned at the desired location. The results are shown in Fig. 3.1.13.

3.1.4. SRMs, instrumentation and data-collection procedures

NIST maintains a suite of SRMs suitable for calibration of powder-diffraction equipment and measurements (NIST, 2015*a*,*b*,*c*,*d*). These SRMs can be divided into various categories based on the characteristic they are best at calibrating for: line position, line shape, instrument response or quantitative analysis, although some degree of overlap exists. The powder SRMs are certified in batches, typically consisting of several kilograms of feedstock, that are homogenized, riffled and bottled prior to the certification. A representative sample of the bottle population, typically consisting of ten bottles, undergoes certification measurements. The specific size of each lot is based on expected sales rates, mass of material per unit and an anticipated re-certification interval of 5 to 7 years. When the stocks of a given certification are exhausted, a new batch of the SRM is certified and a letter is appended to the code to indicate the new certification. Hence SRM 640e (2015) is the sixth certification of SRM 640, originally certified in 1973. The microstructural character of the SRM artifact and/or the certification procedure itself are expected to change (improve) with each renewal.

To understand the role of an SRM in the calibration of XRPD measurements and equipment, it is helpful to discuss briefly the documentation accompanying an SRM [see also Taylor & Kuyatt (1994), GUM (JCGM, 2008*a*) and VIM (JCGM, 2008*b*)]. NIST SRMs are known internationally as certified reference materials. Accompanying an SRM is a certificate of analysis (CoA), which contains both certified and non-certified quantity values and their stated uncertainties. Certified quantity values are determined by NIST to have metrological traceability to a measurement unit – often a direct linkage to the SI. Non-certified values (those lacking the word certified, as presented within a NIST CoA) are defined by NIST as best estimates of the true value provided by NIST where all known or suspected sources of bias have not been fully investigated. Both certified and non-certified quantity values are stated with an accompanying combined expanded (k = 2) uncertainty. Expanded uncertainty is defined as the combined standard uncertainty values for a given certified value multiplied by a coverage factor, k, of 2 and represents a 95% confidence interval for a given value. The combined standard uncertainties are determined by applying standard procedures for the propagation of uncertainty. The distinguishing characteristic of a NIST-certified quantity value is that all known instrumental measurement uncertainties have been considered, including the uncertainties from the metrological traceability chain. NIST defines uncertainties in two contexts: type A and type B. Type A are the random uncertainties determined by statistical methods, for example the standard deviation of a set of measurements. Type B uncertainties are systematic in nature and their extent is usually based on scientific judgment using all relevant information available on possible biases of the experiment. Assessing the technical origin and magnitude of these type-B uncertainties is a dominant part of the NIST X-ray metrology program.

XRPD SRM-certified quantity values are used primarily for calibration of XRPD measurement systems. The calibration data collected on test instruments also contain the two types of errors: random and systematic. It is the systematic measurement errors, or so-called instrument bias, that can be corrected with a calibration. Calibration is a multi-step process. First, certified quantity values are related to test instrument data. This is done by computing, from these values, what would constitute an 'ideal' data set from the 'measurement method' to be calibrated. The 'method' in this case would include the test instrument, its configuration settings and the data-analysis method to be used in subsequent measurements. Then a data set from the SRM is collected and analysed under the conditions of the method. Lastly, a calibration curve is generated by comparing the 'ideal' data set to the measured one. This would establish a correction to the instrument data and yield a calibrated measurement result. For XRPD, this correction has classically taken the form of a calibration function shifting the apparent 2θ indications. There is also the possibility that comparing the 'ideal' instrument response with the observed one indicates a mechanical, optical or electrical malfunction of the instrument. This, of course, requires further investigation and repair, rather than simply applying a calibration curve.

The generation of a calibration curve as just described can be thought of as a 'classical' calibration, and is applicable when the data-analysis procedure(s) use empirical methods to parameterize the observations. More recent, advanced methods such as the FPA use model functions that relate the form of the data directly to the characteristics of the diffraction experiment. The parameters of the model describing the experiment are refined in a least-squares context in order to minimize the difference between a computed pattern and the observed one. With the use of methods that use model functions, the calibration takes on a different form, as the collection and analysis of data can be thought of as replacing the aforementioned multi-step process. The calibration is completed by comparing the results of the refinement with certified quantity values from an appropriately chosen SRM and the known physical-parameter values that describe the optical configuration of the test instrument.

Random measurement error, describing the variation of data for a large set of measurements, can be estimated by repeating measurements over an extended period and computing the variance in the data. Furthermore, over time, one could recalibrate the system and look at the variance of the systematic bias for a given instrument, *i.e.* the rate of drift in the instrument. One would also have to investigate the sensitivity of both the random error and the variance in the systematic bias to environmental variables such as ambient temperature, power fluctuations *etc*. This systematic error variance, combined with the prior determined random error variance and the certified value and its uncertainty, provides an instrumental measurement uncertainty that can be applied to all measurements from a given instrument. Such an in-field study, however, would take years to complete. Instead, the instrumental measurement uncertainties for a given commercial XRPD measurement system are typically provided by the manufacturer, with the stated caveat that periodic calibrations should be performed *via* factory specifications. The instrumental measurement uncertainties determined through such a study are invariably much larger than those of the NIST-certified quantity values, as they contain both the instrument measurement errors (systematic and random) combined with certified quantity value uncertainties.

NIST maintains a suite of more than a dozen SRMs for powder diffraction. However, one often encounters discussions of non-institutionally-certified standards such as 'NAC' ($Na_2Ca_3Al_2F_{14}$), annealed yttrium oxide and silver behenate. Our discussions here

principally concern SRMs 640e (silicon), 660b (NIST, 2010) (lanthanum hexaboride), 1976b (2012) (a sintered alumina disc) and 676a (NIST, 2008) (alumina). SRM 660b has since been renewed as SRM 660c (2014). Most of the work presented here was performed using SRM 660b; however, SRM 660c could be used in any of these applications with identical results. SRMs certified to address the calibration of line position, such as SRMs 640e, 660c and 1976b, are certified in an SI-traceable manner with respect to lattice parameter. SRM 1976b is also certified with respect to 14 relative intensity values throughout the full 2θ range accessible with Cu $K\alpha$ radiation. As such, it is used to verify the correct operation of a diffractometer with respect to diffraction intensity as a function of 2θ angle, *i.e.* instrument sensitivity (Jenkins, 1992) or instrument response. SRM 676a is a quantitative-analysis SRM certified with respect to phase purity (Cline *et al.*, 2011). While SRM 676a is certified for use as a quantitative-analysis SRM, it is also certified with respect to lattice parameters.

Starting with the certification of SRM 640c in 2000, the 640*x* SRMs have been prepared in a way that minimizes sample-induced line broadening. These powders consist of single-crystal particles that were annealed after comminution in accordance to the method described by van Berkum *et al.* (1995). Their crystallite-size distributions (as determined by laser scattering) have a maximum probable size of approximately 4 μm with 10% of the population being above 8 μm and 10% of the population being below 2.5 μm (with trace quantities below 1 μm). With Cu $K\alpha$ radiation, silicon has a linear attenuation of 148 cm^{-1}, which is a relatively low value. SRMs 660*x* consist of lanthanum hexaboride, which was prepared to display a minimal level of both size and microstrain broadening. With the release of SRM 660a, high-resolution diffraction using synchrotron radiation must be used to detect microstructural broadening. However, the use of lanthanum hexaboride by the neutron-diffraction community is problematic, as the naturally abundant isotope ^{10}B has an extremely high neutron absorption cross section. Lanthanum hexaboride made from ^{10}B is essentially opaque to neutrons, rendering it unsuitable for neutron experiments. This problem was addressed with SRMs 660b and 660c by means of a dedicated processing run using a boron carbide precursor enriched with the ^{11}B isotope to a nominal 99% concentration. As such, SRMs 660b and 660c are suitable for neutron experiments; they display a miniscule reduction in microstrain broadening relative to 660a. SRMs 660b and 660c were prepared at the same time using identical procedures and equipment, but in different lots. Lanthanum hexaboride has a relatively high linear attenuation of 1125 cm^{-1} with Cu $K\alpha$ radiation. This linear attenuation virtually eliminates the contribution of specimen transparency to the observed data; as such it offers a more accurate assessment of the IPF for a machine of Bragg–Brentano geometry than is available from other SRMs in the suite. The powders of the SRM 660*x* series consist of aggregates, with the crystallite size being approximately 1 μm and the aggregate size distribution being centred at approximately 8 μm for SRM 660a and 10 μm for 660b and 660c. SRM 676a consists of a fine-grained, equi-axial, high-phase-purity α-alumina powder that does not display the effects of preferred orientation. It consists of approximately 1.5 μm-diameter aggregates with a broad crystallite-size distribution centred at 75 nm. Therefore, the diffraction lines from SRM 676a display a considerable degree of Lorentzian size broadening, with a $1/\cos\theta$ dependence.

SRM 1976b consists of a sintered alumina disc; this format eliminates the variable of sample-loading procedure from the diffraction data collected from this SRM. The alumina powder precursor for SRMs 1976, 1976a and 1976b consists of a 'tabular' alumina that has been calcined to a high temperature, approximately 1773 K. This calcination results in a phase-pure α-alumina powder with a plate-like crystal morphology, approximately 10 μm in diameter by 2 to 3 μm in thickness, leading to the texture displayed by these SRMs. The feedstock for SRMs 1976, 1976a and 1976b was manufactured with a common processing procedure: the compacts are liquid-phase sintered using a 3 to 5% anorthite glass matrix; hot forging was used to achieve a compact of approximately 97% of theoretical density. A unique outcome of the hot-forging operation used to manufacture these pieces was the axi-symmetric texture imparted to the microstructure. This axi-symmetric nature permits mounting of the sample in any orientation about the surface normal. Furthermore, as the sintered compacts cool, the viscosity of anorthite steadily increases, solidifying at approximately 1073 K. This permits intergranular movement during cooling, at least until 1073 K, and reduces the level of microstrain that would otherwise build between the grains due to the anisotropic thermal expansion behaviour of alumina. However, despite this relaxation mechanism, SRM 1976*x* still displays a discernable level of Gaussian microstrain broadening. SRMs 1976a and 1976b were manufactured in a single custom production run, and display a much more uniform level of texture than SRM 1976. This fact is reflected in the considerably smaller uncertainty bounds on the certified relative intensity values of SRMs 1976a and 1976b compared to the original SRM 1976.

Mounting of powder specimens for analysis using Bragg–Brentano geometry is a non-trivial process that typically requires 20 to 30 min. The objective is to achieve a maximum in packing density of the powder with a smooth, flat surface. A 5 μm displacement error in the position of the sample surface will have a noticeable impact on the data collected. Side-drifted mounts allow for realization of a flat surface with relative ease, though maximizing the density of the compact can be challenging. Top-mounted specimens can be compacted using a glass plate or bar that allows the operator to see the sample surface through the glass and, in real time, determine the success or failure in obtaining the desired outcome. Some powders, such as that of SRM 640e, 'flow' in the mount with the oscillation of the glass plate across the sample surface. Others, such as SRM 676a do not flow at all, but can be 'chopped' into the holder and compacted with a single compression. Several attempts may be necessary to realize a high-quality mount. A low-wetting-angle, low-viscosity silicone-based liquid resin, such as those marketed as vacuum-leak sealants for high-vacuum operations, can be used to infiltrate the compact once it is mounted; this results in a stable sample that will survive some degree of rough handling.

The diffractometer discussed in this work is a NIST-built instrument with a conventional optical layout, although it has several features that are atypical of equipment of this nature. It was designed and built to produce measurement data of the highest quality. This outcome is not only consistent with the certification of SRMs, but is also requisite to critical evaluation of modern data-analysis methods (another goal of this work), as discussed below. The essence of the instrument is a superior goniometer assembly that is both stiff and accurate in angle measurement, in conjunction with standard but thoroughly evaluated optics. The tube shield and incident-beam optics are mounted on a removable platform that is located *via* conical pins that constitute a semi-kinematic mount. This feature allows rapid interchange between various optical geometries. Fig. 3.1.23 shows

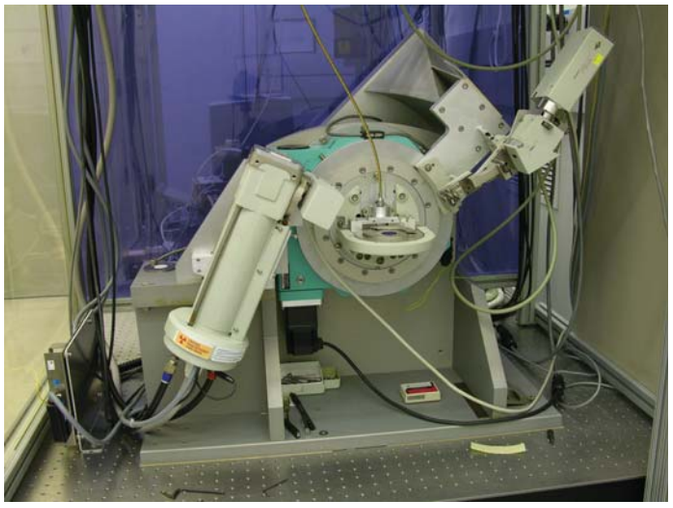

Figure 3.1.23
The X-ray powder diffractometer designed and fabricated at NIST, in conventional divergent-beam format.

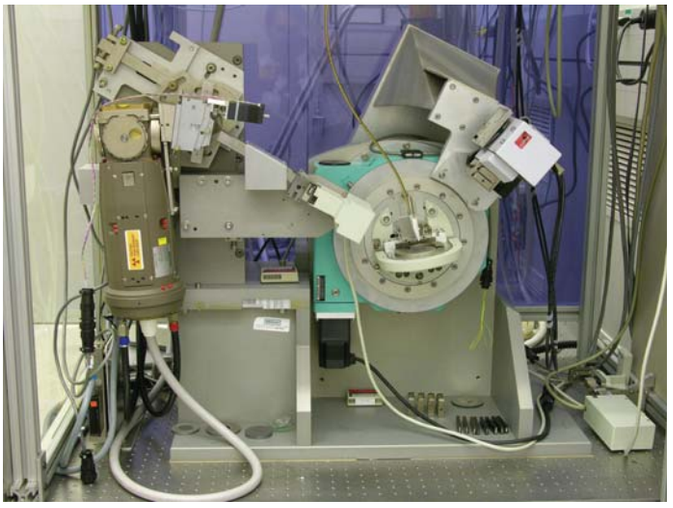

Figure 3.1.24
The NIST-built powder diffractometer configured with the Johansson incident-beam monochromator and a position-sensitive detector.

the instrument set up in conventional geometry with a post-monochromator and point detector, while Fig. 3.1.24 shows the setup with a Johansson IBM and a PSD. Data from these two configurations are discussed below.

The goniometer assembly, which is of θ–2θ geometry, uses a pair of Huber 420 rotation stages mounted concentrically with the rotation axes horizontal. The stage that provides the θ motion faces forward while the 2θ stage faces rearward; they are both mounted on a common aluminium monolith, visible in Figs. 3.1.23 and 3.1.24, which forms the basis of the chassis for the instrument. Both stages incorporate Heidenhain 800 series optical encoders mounted so as to measure the angle of the ring gear. With 4096-fold interpolation provided by IK220 electronics, an angle measurement to within $\pm 0.00028^\circ$ (1 arc second) was realized for both axes. The stages are driven by five-phase stepper motors that incorporate gear reducers of 10:1 for the θ stage and 5:1 for the 2θ stage, yielding step sizes of 0.0002° and 0.0004°, respectively. The manufacturer's specifications for the Huber 420 rotation stage claim an eccentricity of less than 3 μm and a wobble of less than 0.0008° (3 arc seconds). The construction of the goniometer assembly necessitated the development of a specialized jig to align the two 420 rotation stages with regard to both the concentricity (eccentricity) and parallelism (wobble) of their rotation axes. The result was that the overall eccentricity and wobble of the assembly met the specifications cited for the individual stages. The flexing of the detector arm, attached to the rearward-facing 2θ stage, was minimized by fabricating a honeycombed aluminium structure, 7.6 cm deep, which maximized stiffness while minimizing weight. Furthermore, the entire detector-arm assembly, including the various detectors, was balanced on three axes to minimize off-axis stress on the 2θ rotation stage (Black *et al.*, 2011). Thus, the goniometer assembly is exceedingly stiff and offers high-accuracy measurement and control of both the θ and 2θ angles.

The optics, graphite post-monochromator, sample spinner, X-ray generator and tube shield of the machine were originally components of a Siemens D5000 diffractometer, *circa* 1992. As previously discussed, the parts for the IBM configuration were obtained primarily from a Siemens D500, *circa* 1987. Both configurations include a variable-divergence incident-beam slit from a D5000. The PSD used in this work was a Bruker LynxEye XE. The cable attached to the sample spinner (as seen in Figs. 3.1.23 and 3.1.24) is a flexible drive for the spinner itself; the remote location of the drive motor (not shown) isolates the sample and machinery from the thermal influence of the motor. The machine was positioned on an optical table within a temperature-controlled (± 0.1 K) space. The temperature of the water used for cooling the X-ray tube and generator was regulated to within ± 0.01 K. Operation of the machine was provided through control software written in *LabVIEW*. Data were recorded in true x–y format using the angular measurement data from the optical encoders.

In conventional configuration, the 2.2 kW copper tube of long fine-focus geometry was operated at a power of 1.8 kW. This tube gives a source size of nominally 12×0.04 mm, while the goniometer radius is 217.5 mm. The variable-divergence slit was set to $\sim 0.9^\circ$ for the collection of the data discussed here. This results in a beam width, or footprint at the lowest θ angle, on the sample of about 20 mm, conservatively smaller than the sample size of 25 mm. A Soller slit with a divergence of 4.4° defined the axial divergence of the incident beam. A 2 mm anti-scatter slit was placed approximately 113 mm in front of the 0.2 mm (0.05°) receiving slit. The total path length of the scattered radiation (the goniometer radius plus the traverse through the post-monochromator) was approximately 330 mm. This setup reflects what is thought to be a medium-resolution diffractometer that would be suitable for a fairly broad range of applications and is therefore a reasonable starting point for a study of instrument calibration. With the IBM, the 1.5 kW copper tube of fine-focus geometry was operated at a power of 1.2 kW. This tube had a source size of nominally 8×0.04 mm. The variable-divergence incident slit was also set to 0.9° with a 0.2 mm (0.05°) receiving slit. The receiving optics were fitted with a 4.4° Soller slit. The total beam-path length was about 480 mm.

With the scintillation detector, data were collected using two methods, both of which encompassed the full 2θ range available with these instruments and for which the SRMs show Bragg reflections. The first involves data collection in peak regions only, as illustrated in Table 3.1.2 for SRM 660b. The run-time parameters listed in Table 3.1.2 reflect the fact that the data-collection efficiency can be optimized by collecting data in several regions, as both the intensity and breadth vary systematically with respect to 2θ. This was the manner in which data were collected for the certification measurements of SRMs 660c, 640e and 1976b. The

Table 3.1.2
Run-time parameters used for collection of the data used for certification of SRM 660b

The 'overhead time' associated with the operation of the goniometer is included.

hkl	Start angle (°)	End angle (°)	Step width (°)	Count time (s)	Total peak time (min)
100	20.3	22.2	0.01	2	6.3
110	29.1	31.4	0.01	1	3.8
111	36.4	38.4	0.01	3	10.0
200	42.7	44.4	0.01	5	14.2
210	48	50	0.008	2	8.3
211	53.2	54.896	0.008	5	17.7
110	62.5	64.204	0.008	11	39.0
300	66.7	68.596	0.008	4	15.8
310	70.9	72.7	0.008	6	22.5
311	75	76.904	0.008	9	35.7
222	79.3	80.804	0.008	47	147.3
320	83	84.904	0.008	15	59.5
321	86.9	88.9	0.008	8	33.3
400	95	96.704	0.008	42	149.1
410	98.6	100.8	0.008	9	41.3
330	102.7	104.9	0.008	12	55.0
331	106.9	108.9	0.01	27	90.0
420	111.1	113.1	0.01	20	66.7
421	115.3	117.6	0.01	10	38.3
332	119.9	122.1	0.01	19	69.7
422	129.6	131.796	0.012	32	97.6
500	134.9	137.396	0.012	27	93.6
510	140.5	144	0.014	7	29.2
511	147.5	150.908	0.016	15	53.2
					Total time = 20.0 hours

second involved a simple continuous scan of fixed step width and count time. It is generally accepted that a step width should be chosen so as to collect a minimum of five data points above the full-width-at-half-maximum (FWHM) to obtain data of sufficient quality for a Rietveld analysis (Rietveld, 1967, 1969; McCusker *et al.*, 1999). This does not, however, constitute any sort of threshold; collecting data of a finer step width can, with proper data analysis, result in a superior characterization of the IPF. However, one must consider the angular range of acceptance of the receiving slit that is chosen. For a slit of 0.05° a step width of 0.005° would add only 10% 'new' information, so selecting this step width would not be worth the extra data-collection time. We did, however, collect some data sets we refer to as 'ultra-high-quality' data; the step widths for these were half those shown in Table 3.1.2 and the count times were approximately three times higher than those in Table 3.1.2. For the reported instrument and configuration, the run-time parameters of Table 3.1.2 result in a minimum of 8 to 10 points above the FWHM. Count times were selected to obtain a uniform number of counts for each profile. It should be noted that it is probably not worth spending time collecting quality data from the 222 line of LaB_6, as it is of low intensity and relatively close to other lines of higher intensity; however, this is not the case with the 400 line. Selection of the run-time parameters can be an iterative process; the total width of each profile scan was set to include at least 0.3° 2θ of apparent background on either side of the profile. Except for the data for SRM 676a, the continuous scans discussed were collected with a step width of 0.008° 2θ and a count time of 4 s to result in a scan time of roughly 24 h. The scans of 676a were collected with 0.01° 2θ step width and 5 s count time.

The PSD used on the NIST diffractometer was a one-dimensional silicon strip detector operated in picture-taking mode for all data collection. It has an active window length of 14.4 mm that is divided into 192 strips for a resolution of 75 µm. With a goniometer radius of 217.5 mm this constitutes an active angular range of 3.80° with 0.020° per strip. Slits that would limit the angular range of the PSD window were not used; with each step the counts from all 192 channels were recorded. The PSD was stepped at 0.005° 2θ, for 25% new information per strip; however, to reduce the data-collection time a second coarse step was also included. Therefore, the data-collection algorithm includes the selection of three parameters: a fine step of 0.005°, the number of fine steps between coarse steps (4), and the size of a coarse step (typically 0.1° or 0.2° 2θ). This approach allows for the collection of high-resolution data without stepping through the entire pattern at the high-resolution setting. Data were collected with four fine steps per detector pixel and a coarse step of 0.1° 2θ. They were processed to generate x–y data for subsequent analysis. The operator can select the portion of the 192 channels, centred in the detector window, to be included in the generation of the x–y file. The PSD was fitted with a 1.5° Soller slit for collection of the data presented here.

3.1.5. Data-analysis methods

Data-analysis procedures can range from the entirely non-physical, using arbitrary analytical functions that have been observed to yield reasonable fits to the observation, to those that exclusively use model functions, derived to specifically represent the effect of some physical aspect of the experiment. The non-physical methods serve to parameterize the performance of the instrument in a descriptive manner. The origins of two of the most common measures of instrument performance are illustrated in Fig. 3.1.25. The first is the difference between the apparent position, in 2θ, of the profile maximum and the position of the Bragg reflection computed from the certified lattice parameter. These data are plotted *versus* 2θ to yield a $\Delta(2\theta)$ curve; a typical example is shown in Fig. 3.1.26. An illustration of the half-width-at-half-maximum (HWHM), which is defined as the width of either the right or left half of the profile at one half the value of maximum intensity after background subtraction, is also shown in Fig. 3.1.25. These values can be summed to yield the FWHM, and plotted *versus* 2θ to yield an indication of the profile breadth as it varies with 2θ (Fig. 3.1.27). In addition, the left and right HWHM values of Fig. 3.1.28 gauge the variation of profile asymmetry with 2θ; additional parameters of interest, such as the degree of Lorentzian and Gaussian contribution to profile shape,

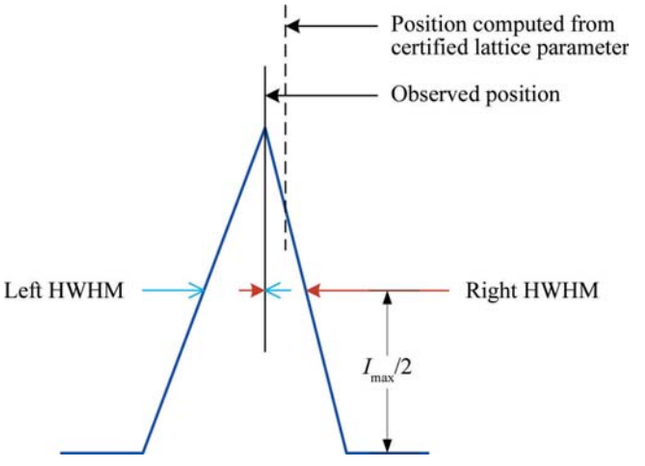

Figure 3.1.25
Diagrammatic representation of a powder-diffraction line profile, illustrating the metrics $\Delta(2\theta)$ and half-width-at-half-maximum (HWHM). The full-width-at-half-maximum (FWHM) = left HWHM + right HWHM.